

A nonlinear model for a three-phase 12/8 switched reluctance machine

Dimitar Kirov Yankov, Tsvetana Grigorova Grigorova

Department of Electronics, Faculty of Electronics and Automation, Technical University of Sofia, Plovdiv Branch, Bulgaria

Article Info

Article history:

Received Feb 22, 2022

Revised May 25, 2022

Accepted Jun 7, 2022

Keywords:

Generating mode

Modeling

Motoring mode

SRM nonlinear model

Switched reluctance motor

ABSTRACT

The paper presents a methodology for the synthesis of a nonlinear model for a three-phase 12/8 switched reluctance machine (SRM) in a MATLAB/Simulink environment. The required switched reluctance motor characteristics are derived using the finite element analysis (FEA). Graphical and tabular results of the relations flux/current/position, current/torque/position, and inductance/current/position used to create the SRM model are presented. The structure of the nonlinear three-phase 12/8 SRM model is discussed and its implementation in Simulink is presented. A series of simulation and experimental results are performed to verify the accuracy of the built three-phase, 12/8 SRM (H55PWBKM-1844) nonlinear model. A very good alignment between simulation and experimental results is observed.

This is an open access article under the [CC BY-SA](https://creativecommons.org/licenses/by-sa/4.0/) license.



Corresponding Author:

Dimitar Kirov Yankov

Department of Electronics, Faculty of Electronics and Automation, Technical University of Sofia

Plovdiv Branch, 63 Sankt Petersburg Blvd, 4000 Plovdiv, Bulgaria

Email: d.yankov@tu-plovdiv.bg

1. INTRODUCTION

Switched reluctance machines (SRMs) are characterized by many advantages such as: a simple design, a wide range of possibilities for optimizing the operating modes when changing the speed and load (a possibility to adjust the output parameters of the electric drive), the overload torque capability, a high energy efficiency, reliability and low-cost, which are the reasons that make them considered as promising electromechanical devices [1], [2]. A complete summary of their performances, control methods and other capabilities can be found in [3]. The complexity of modern electric drive systems increases the need to use simulation methods for analysis and optimization based on various computer-aided design systems. Their use allows for determining the permissible deviations of the values of various parameters and control signals in electric drive systems from their calculated values so that the electric drive maintains its efficiency [4].

A powerful tool for an effective design, study and control of an SRM is modelling with a MATLAB/Simulink environment. SRM models are divided into two main categories-linear and nonlinear models [5]. Linear models are applicable when the motor assumes to remain magnetically unsaturated during operation. Furthermore, the phase inductances change linearly from the rotor position. Linear models of three-phase 6/4 SRM and three-phase 12/8 SRM are demonstrated in [5]-[7]. These models combine the ability to obtain acceptable results with minimal simulation time. However, the accurate analysis of SRM performance requires precision modelling of the behavior of this motor with its nonlinear magnetic characteristics. The built-in nonlinear models in the MATLAB/Simulink environment are types 6/4, 8/6 and 10/8 SRM [8]. The nonlinear models of other types of SRMs are not included in the Simulink libraries.

The three-phase 6/4 SRM has two magnetic poles per phase, while the three-phase 12/8 SRM has four. The electrical cycle of 6/4 SRM corresponds to a 90° rotation of the rotor position, while the electrical

cycle of 12/8 SRM corresponds to a 45° rotation. Besides, when the speed of 12/8 SRM is equal to half of 6/4 SRM speed, the inductance cycles of both machines are equal. The turn-on and turn-off angles of the 12/8 SRM are half of the same angles at 6/4 SRM. In addition, [9] discuss the possibility of modelling in Simulink the three-phase 12/8 SRM by modifying the existing model of the three-phase 6/4 SRM.

Furthermore, the existing SRM model can be modified directly, or a new model can be added to the model library [9]. However, this approach does not allow to precisely model the behaviour of a specific type of 12/8 SRM. It should be noted that the flux linkage profile and the torque profile are changed with current and position. Besides, when operating at higher phase currents, the change with current is nonlinear.

The method for structuring a nonlinear model of SRM considered in [10] allows the user to create their model with the ability to set multiple input parameters and implement nonlinear static characteristics. The initial data for the proposed model are the relationship of flux linkage as a function of position and the phase current. The necessary values of the current depending on the position and flux linkage and the torque depending on position and current are received, solving the corresponding differential equations. The use of partial derivatives should be avoided because they can become a source of error [5]. The waveforms obtained during simulations are not verified experimentally.

Saidani and Ghariani [11], presented the results from the modelling of 12/8 SRM. The flux linkage curve is prepared through coupled to MATLAB FEMM simulation for different rotor positions and then is used to extract the other performance as static torque, inductance and co-energy. The look-up table, developed in the form of a block in the Simulink model, is obtained through MATLAB/Simulink. The simulation results are not confirmed with an experiment. The presented nonlinear models in [12]-[14] describe methods for structuring an SRM nonlinear model. These models use extensive analytical calculations and partial derivative calculations. Polynomial interpolation is also used. Thus, they emphasize the computational time of SRM simulations and the accuracy of the flux linkage partial derivative. These methods do not allow easy synthesis of an SRM model.

The nonlinear model presented in [15] uses the data obtained from measurements of the static characteristics of the motor. They were implemented in the form of 2D tables in the MATLAB/Simulink environment. Disadvantages of the considered model are: a missing detailed description for structuring the model; a menu for setting the basic parameters of the studied motor; a method by which the data obtained from measurements are introduced into the model. The main disadvantages of the experimentally obtained static characteristics for magnetization and torque of the motor are the lack of precision in the measurement and the inability to stop the rotor at high currents without minimal slippage. To perform a simulation study to another type of SRM, it is necessary to provide the user with the capability to create their specific model based on catalogue data and the same time, save the computational time of SRM simulations.

The present study presents a methodology for synthesising a custom nonlinear model of three-phase 12/8 SRM in the Simulink environment. The procedure we used with MATLAB/Simulink is based on creating look-up tables that approximate the necessary relations. For this purpose, the approach given in [5] is applied. The required SRM characteristics of the tested 12/8 SRM are modelled by a FEM, as demonstrated in [16], providing us with the different magnetic data to realise the look-up tables. Thus, the used procedure allows avoiding all partial derivatives. The data for the look-up tables in excel files are entered using the source code for reading data in the Simulink software simulator. The individual blocks for structuring a proposed nonlinear model in MATLAB/Simulink are described step by step.

2. MATHEMATICAL DESCRIPTION OF THE SRM NONLINEAR MODEL

The expression of the phase voltage for a one phase of the SRM, describing the dynamic behaviour of the SRM, while assuming that there is no mutual coupling to other phases, is given by [1]:

$$V_{ph}(t) = i_{ph}(t) \cdot R_{ph} + \frac{d\lambda_{ph}(i_{ph}, \theta_{ph})}{dt}, \quad (1)$$

where V_{ph} is the voltage applied to the terminals of one phase, i_{ph} is the phase current, R_{ph} is the resistance per phase, $\lambda_{ph}(i_{ph}, \theta_{ph})$ is the flux linkage per phase at different excitation currents and rotor positions θ_{ph} . The flux linkage in an SRM phase is given by:

$$\lambda_{ph} = L_{ph}(i_{ph}, \theta_{ph}) \cdot i_{ph}, \quad (2)$$

where $L_{ph}(i_{ph}, \theta_{ph})$ shows the dependence of the phase inductance on the rotor position and the excitation current. The torque produced by one phase T_{ph} can be approximated by:

$$T_{ph}(i_{ph}, \theta_{ph}) = \int_0^{i_{ph}} \frac{\partial \lambda_{ph}(i_{ph}, \theta_{ph})}{\partial \theta_{ph}} di_{ph}, \quad (3)$$

the total electromagnetic torque for the SRM with 3-phases is given by:

$$T_e = \sum_{j=1}^3 T_{phj}(i_{phj}, \theta_{phj}), \quad (4)$$

where j is the phase number. The following mechanical equations were used to obtain the output speed of an SRM:

$$J \frac{d\omega}{dt} = T_e - T_{load} - F\omega, \quad (5)$$

$$\omega = d\theta/dt, \quad (6)$$

where J is the machine inertia, T_{load} is the load torque, F is the friction coefficient and ω is the rotor speed of the SRM.

2.1. The nonlinear SRM model

This section presents the model synthesis using some of the techniques described in [10] and the embedded models in Simulink. The required static characteristics are obtained by the finite element method (FEM) [16]-[20]. The mathematical model of the SRM is divided into electrical and mechanical parts. The electrical part is represented by in (1) and (2), while the mechanical part is represented by in (3)-(6).

Creating an adequate nonlinear mathematical model requires considering the highly nonlinear characteristics of the motor such as the inductance, the flux linkage and the torque. For this reason, these dependencies are presented in the two-dimensional tables (look-up tables) at different rotor positions and discrete values of the currents through the phases. The required SRM characteristics are built with the Infolytica MotorSolve software. The modern software for the finite element analysis FEM analysis is characterized with high accuracy and also includes an extensive database of materials from magnets, steels and conductors with measured values of properties provided by their manufacturers. The MotorSolve software simulates machine performance using equivalent circuit calculations and a unique automated finite element analysis machine [21]. Several analysis methods are included in this platform, which give the user control of the accuracy versus time.

2.1.1. The SRM operational characteristics and inductance profile

As the first step, a set of relations flux/current/position, current/torque/position, and inductance/current/position are necessary to create the model. The graphical representation of the results for the flux linkages dependence $\lambda_{ph}(i_{ph}, \theta_{ph})$, obtained after the FEM analysis for the tested three-phase 12/8 SRM, is shown in Figure 1. The flux linkage values obtained by the FEM correspond to 90 rotor positions from 0° to 45° (at resolution of 0.5°) and 100 different values of the current from 0 to 20 A (current resolution of 0.2 A).

The next characteristic is the inductance profile $L_{ph}(i_{ph}, \theta_{ph})$. Using FEM tools, the dependence of the inductance versus rotor position of the used three-phase 12/8 SRM for different excitation currents is derived. The obtained results for the phase inductance, displayed in Figure 2, correspond to 90 rotor positions from 0° to 45° (at resolution of 0.5°) and 99 different values of the current from 0.2 to 20 A (current resolution of 0.2 A).

The most challenging task is the construction of the flux data $\lambda_{ph_FEM}(i_{ph}, \theta_{ph})$ since the model calculates the current as a function of flux and position $i_{ph}(\lambda_{ph_FEM}, \theta_{ph})$. Hence, it is necessary to process and rearrange the data $\lambda_{ph_FEM}(i_{ph}, \theta_{ph})$ to produce the required current $i_{ph}(\lambda_{ph_FEM}, \theta_{ph})$. The graphical representation for the set of curves $i_{ph}(\lambda_{ph_FEM}, \theta_{ph})$ in the Infolytica MotorSolve is presented in Figure 3. The obtained values correspond to 90 rotor positions from 0° to 45° (at resolution of 0.5°). It should be noted that the data for the flux linkages dependence $\lambda_{ph_FEM}(i_{ph}, \theta_{ph})$ and the inductance profile $L_{ph_FEM}(i_{ph}, \theta_{ph})$ corresponds to the values for one phase. Because the study assumes there is no mutual coupling between the phases, the look-up tables used to for one phase are also used to model all phases.

The dependencies of the torque produced by one phase as a function of rotor position and phase current values $T_{ph}(i_{ph}, \theta_{ph})$ are shown in Figure 4. The obtained results correspond to 90 rotor positions from 0° to 45° (at resolution of 0.5°) and 100 different values of the current from 0 to 20 A (current resolution of 0.2 A). The obtained graphs and numerical results correspond to the operation of the SRM in motoring and generating mode. In addition, the results show the influence of the nonlinearity of the magnetization characteristic on the phase torque.

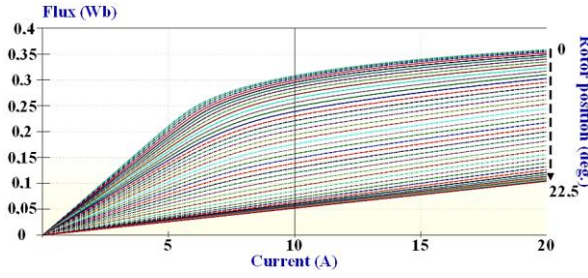


Figure 1. Infolytica MotorSolve 2D flux linkages vs current characteristics of the tested three-phase 12/8 SRM at resolution of 0.5

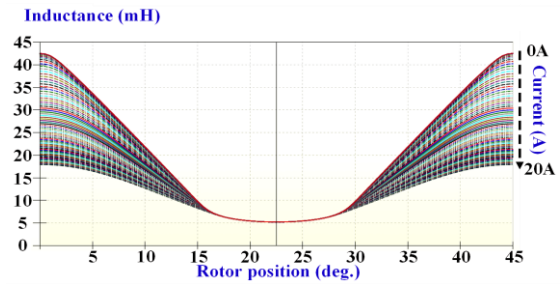


Figure 2. Infolytica MotorSolve 2D inductance vs rotor position characteristics of the tested three-phase 12/8 SRM for different excitation currents

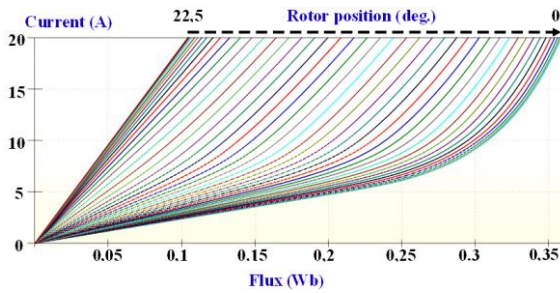


Figure 3. Infolytica MotorSolve 2D i_{ph} ($\lambda_{ph_FEM}, \theta_{ph}$) characteristics of the tested three-phase 12/8 SRM at resolution of 0.5°

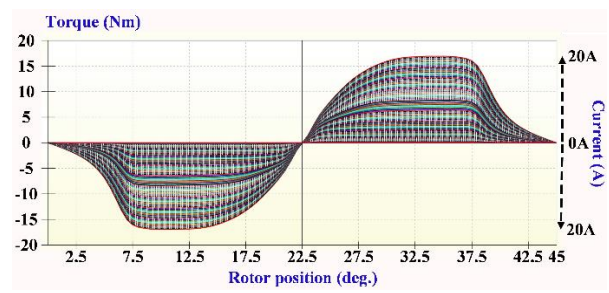


Figure 4. Infolytica MotorSolve 2D phase torque vs current characteristics of the tested three-phase 12/8 SRM at resolution of 0.5

2.1.2. The implementation of the SRM nonlinear model in Simulink

The schematic diagram of the SRM nonlinear model implemented in MATLAB/Simulink environment is presented in Figure 5. The block named source includes the conventional blocks used for the implementation of in (1)-(6) and the nonlinear characteristics of the motor, receiving from FEM. The simulation of each motor phase is realized using the blocks named phase (phase A, phase B and phase C). The approach in [10] is used.

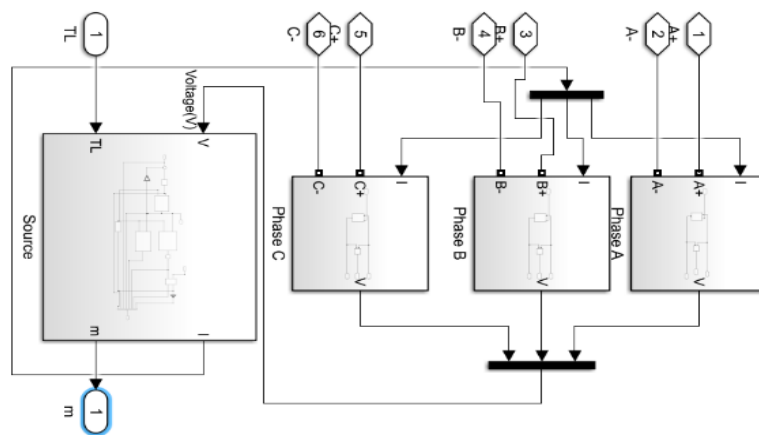


Figure 5. The structure of the nonlinear three-phase 12/8 SRM model

Figure 6 shows the internal structure of the block named source. It contains the three look-up-tables denoted as 2-D lookup current ($i_{ph}(\lambda_{ph_FEM}, \theta_{ph})$), 2-D lookup inductance ($L_{ph_FEM}(i_{ph}, \theta_{ph})$), 2-D lookup torque ($T_{ph}(i_{ph}, \theta_{ph})$), the block for calculating the total torque and the rotor position block (position_rotor).

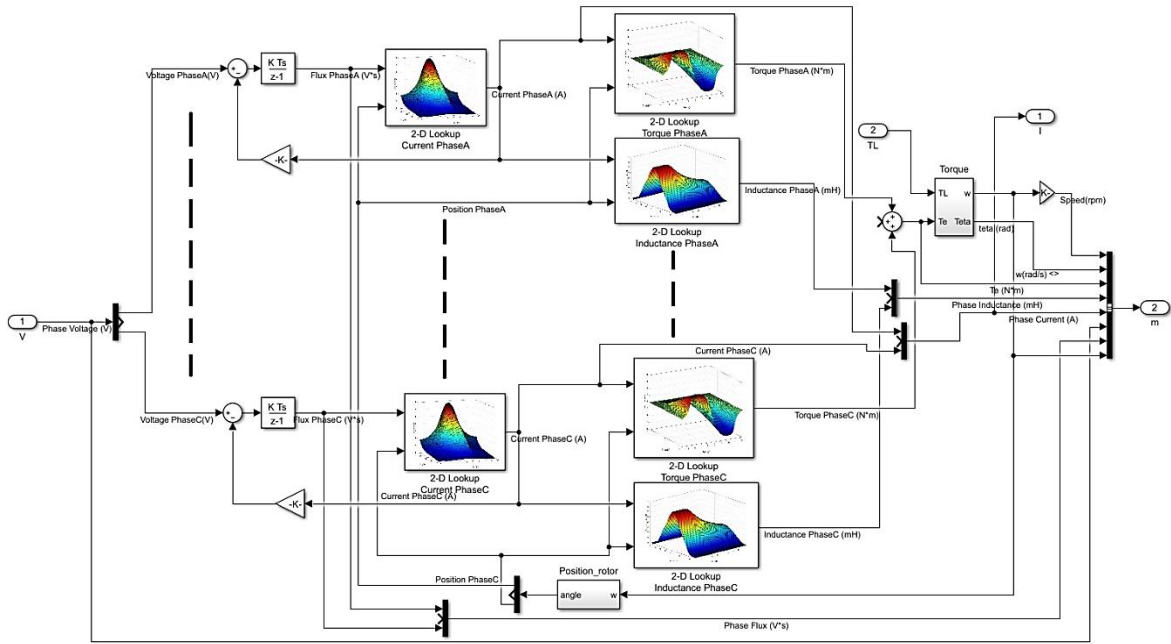


Figure 6. The block source schematic diagram

The data for the two-dimensional tables (2-D lookup tables) in excel files are entered using the source code for reading data in the simulink software simulator in the PostLoadFcn menu. Snapshots of the PostLoadFcn menu with part of the code and the user interface, where the values for the current are entered, for the creation of the respective block 2D-Lookup table are shown in Figure 7 and Figure 8.

The block denoted as Torque implements the mechanical in (4)-(6). Figure 9 illustrates their internal structures. The input data are the signals of the load torque T_L and the total torque T_e , which determine the rotor speed ω and the magnitude of the rotor position $Teta$. The internal structure of the rotor position block is shown in Figure 10. In this block, the rotating speed is integrated, and as a result, the angular position of the rotor for three phases is obtained. The block named phase A (phase B, phase C) includes a current source and a resistor connected in parallel, modelling the phase active resistance. The phase current, derived from the differential equation, is fed to input I of block phase A. Its output signal produces the voltage applied to the phase.

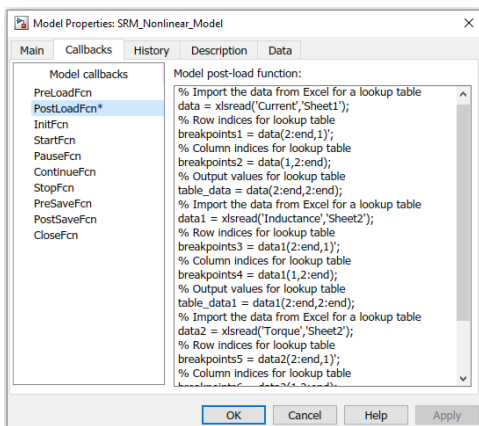


Figure 7. PostLoadFcn menu with source code part for reading data received from FEM analysis

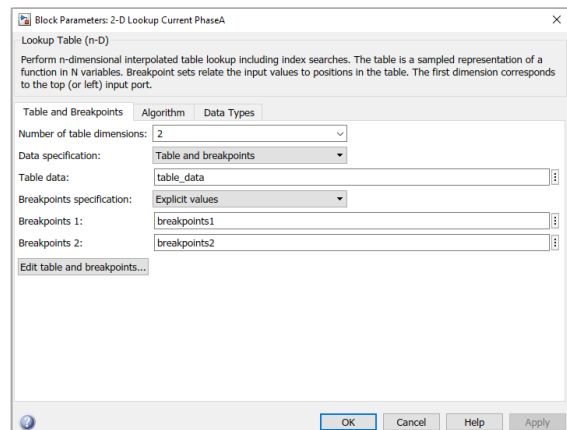


Figure 8. The user interface for entering FEM simulation results on the corresponding table

The tested SRM is fed from the asymmetric bridge converter. This topology is the most widely used in SRM drives in terms of converter losses and cost, control performance, the independent phase windings,

allowing a fault-tolerant operation capability [7]. Hence, for example, the terminals named "A+" and "A-" (block phase A) connect the motor phase A to the corresponding bridge of the asymmetric converter circuit.

The final synthesis of the three-phase 12/8 SRM nonlinear model includes the creation of a subsystem (block subsystem), shown in Figure 11, where the user interface (mask) sets the necessary input parameters such as a phase resistance (Ω), a friction coefficient (N.m.s) and inertial value (kg.m.m). In addition, by checking the plot magnetization curves field of the subsystem, the flux linkages dependencies are displayed as shown in Figure 12.

Figure 13 presents the schematic diagram used to simulate in MATLAB/Simulink the proposed nonlinear three-phase 12/8 SRM model. It consists of the following main blocks: block SRM 12/8 (nonlinear SRM model), block converter, block position_sensor, monitoring the position of the rotor and switching the phase transistors. The internal circuit of the phase bridge A of the asymmetric converter is shown in Figure 14.

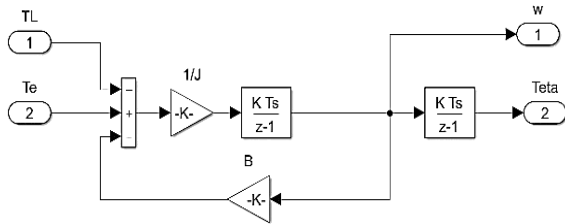


Figure 9. Internal structure of the mechanical block of the SRM for determining the Theta and rotor speed ω

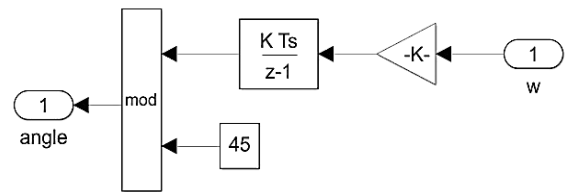


Figure 10. Internal structure of the block for the rotor position

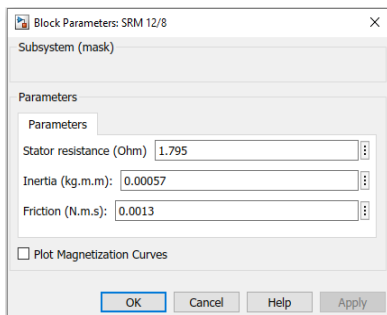


Figure 11. The user interface for custom parameters definition

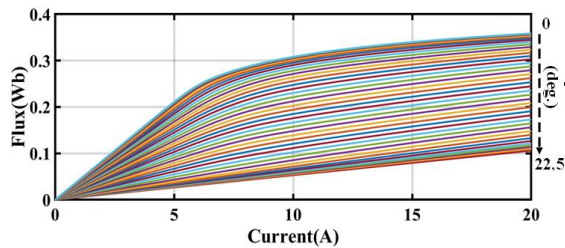


Figure 12. MATLAB/Simulink 2D flux linkages vs current characteristics of the tested three-phase 12/8 SRM at resolution of 0.5°

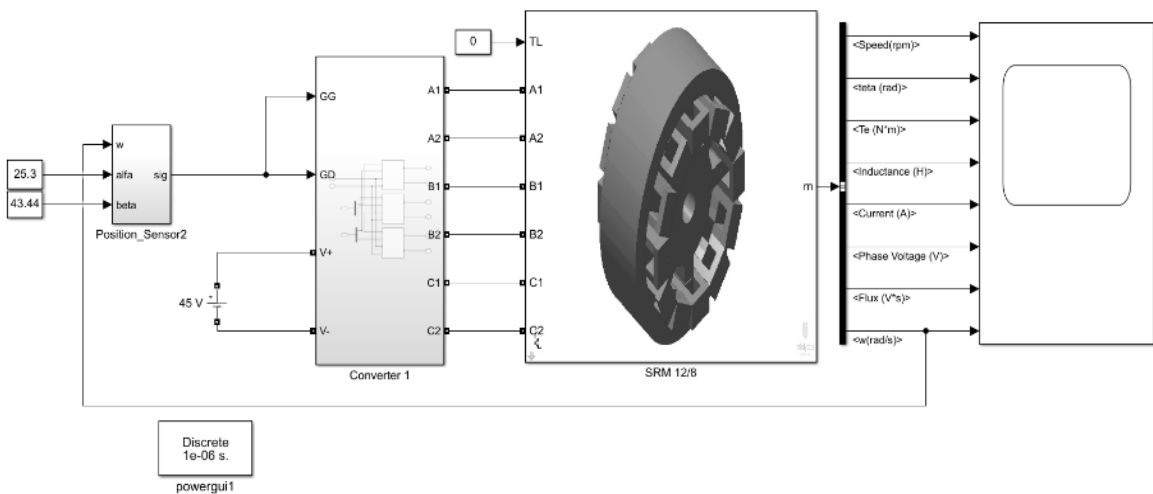


Figure 13. The MATLAB/Simulink schematic diagram for the nonlinear three-phase 12/8 SRM model

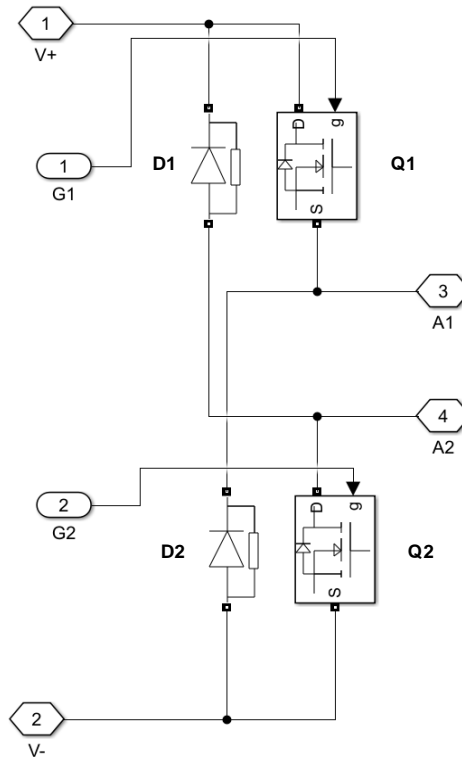


Figure 14. H-bridge asymmetric converter – bridge phase A

The input parameters are as follows: input voltage for motoring $V=45$ V and generating mode $V=8$ V; phase resistance $R_{ph}=1.795$ Ω , inertial value $J=0.00057$ [kg.m.m], friction coefficient $F=0.0013$ [N.m.s], the used MOSFETs are IRFP460 with the following parameters: drain-source on-resistance $R_{DS(on)}=0.24$ m Ω , body diode on-resistance $R_d=0.01$ Ω , body diode voltage $V_{SD}=1.8$ V; the asymmetric bridge diodes are FR604-max. forward voltage $V_F=1.3$ V. Table 1 shows the specification of the tested three-phase switched reluctance motor type 12/8 model - H55PWBM-1844.

Table 1. Specification of tested three-phase 12/8 SRM

Parameters of switched reluctance motor model H55PWBM-1844							
Parameters	Symbol	Value	Units	Parameters	Symbol	Value	Units
Number of phases	Nph	3	-	Inductance aligned position (measured at 0.2 A)	La	42.55	mH
Number of stator poles	Ns	12	-	Inductance unaligned position (measured at 0.2 A)	Lu	5.22	mH
Number of rotor poles	Nr	8	-	inertia	J	0.00057	kg.m.m
Phase resistance	Rph	1,795	ohms	friction coefficient	F	0.0013	N.m.s
Max. current per phase	Iphmax	5.5	amperes	Rated speed	n	1500	rpm/min
Phase voltage	Vph	120	volts	rotor arc angle	β_r	15.5	deg.
Power delivered	P	660	watts	stator arc angle	β_s	15	deg.

3. RESULTS AND DISCUSSION

In this section we proposed the performed simulation and experimental results. To verify the built nonlinear model accuracy, the series of simulation and experimental results are accomplished. The tested SRM is fed from the asymmetric bridge converter. Primarily, the results of the FEM analysis for the inductance profile are compared with those obtained experimentally. For this purpose, the current saturation method for SRM inductance measurement proposed in [22] is applied. The method uses low frequency and low voltage to minimize iron losses; no additional specific devices are needed; the setup is not complicated and compared to classic methods [23]-[27], a higher accuracy of the inductance profile measurement is achieved. Figure 15 shows the simulation and experimental verification of the inductance profile at various excitation currents for the tested three-phase 12/8 SRM.

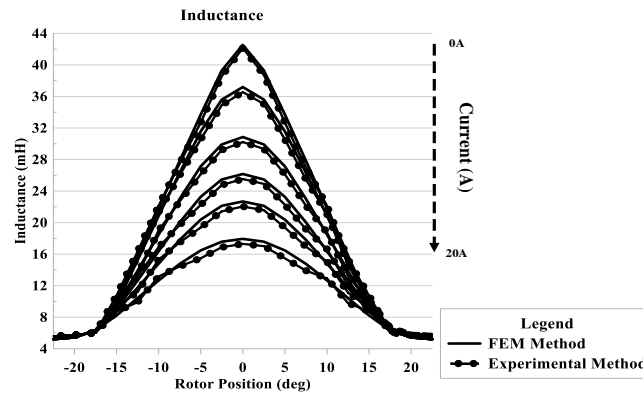


Figure 15. Simulation and experimental verification of the inductance profile L_{ph} at various excitation currents for the tested three-phase 12/8 SRM (H55PWBKM-1844)

A very good alignment between simulation and experimental results is observed. In the present study, to confirm the accuracy of the built three-phase 12/8 SRM nonlinear model, the machine is energized using a voltage source control method. The operation of the motor is examined in quadrants I and II at motor speed $n=1500$ rpm. At the moment when the positive voltage (V_+) feeds to one phase and the motor starts to rotate, the two MOSFETs (Q_1 , Q_2) shown in Figure 14 must be on. Conversely, when the applied voltage has a negative value (V_-), the two diodes (D_1 , D_2) are used to ensure a continuous current mode [1]. The proposed nonlinear model is verified experimentally. Figure 16(a) presents a built three-phase asymmetric bridge converter with the controller. The measuring stand for experimental study of the operation of the three-phase 12/8 SRM with position and torque sensors is shown in Figure 16(b).

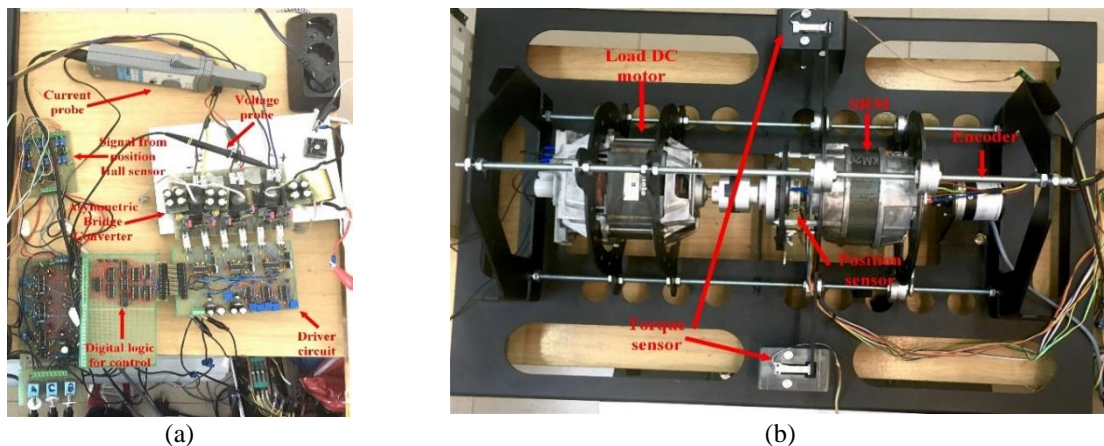


Figure 16. Experimental study: (a) three-phase asymmetric bridge converter with the controller and (b) the measuring stand with position and torque sensors

Depending on the operating mode and the direction of the motor rotation, there are different turn-on and turn-off angles of the motor phases. The oscillograms shown in the following figures correspond to motoring and generating mode, respectively, i.e. the operation in the first and second quadrants. Hence, the turn-on and turn-off angles must be selected in the rising and falling phase inductance for motoring and generating mode. Figure 2 shows that these areas are between 22.5° and 45° for first quadrant and 0° and 22.5° for second quadrant. Therefore, to ensure a rapid increase and decrease of the phase current, it is necessary switching the applied phase voltage in these areas, leading angles corresponding to the minimum and maximum phase inductance (or 22.5° and 45°) for motoring mode and maximum and minimum phase inductance (or 0° and 22.5°) for generating mode. After comparing the voltages and currents of the tested SRM during operation in the I quadrant (motoring mode), the operation of the SRM in the II quadrant (generating mode) was checked by using a collector machine for the motor. During the simulation, load torque $T_L=0.65$ Nm and the motor speed $n=1500$ rpm were specified.

Figure 17(a) illustrates from top to bottom the simulation waveforms of the one-phase voltage and the one-phase current at $\theta_{on} = 25.3^\circ$, $\theta_{off} = 43.44^\circ$, torque load TL=0 Nm and speed n=1500 rpm for the motoring mode (I quadrant). Figure 17(b) illustrates the simulation waveforms of the same quantities - from top to bottom waveforms of the one-phase voltage and the one-phase current at $\theta_{on} = 3.8^\circ$, $\theta_{off} = 20.944^\circ$, torque load TL=0.65 Nm and speed n=1500 rpm for the generating mode (II quadrant).

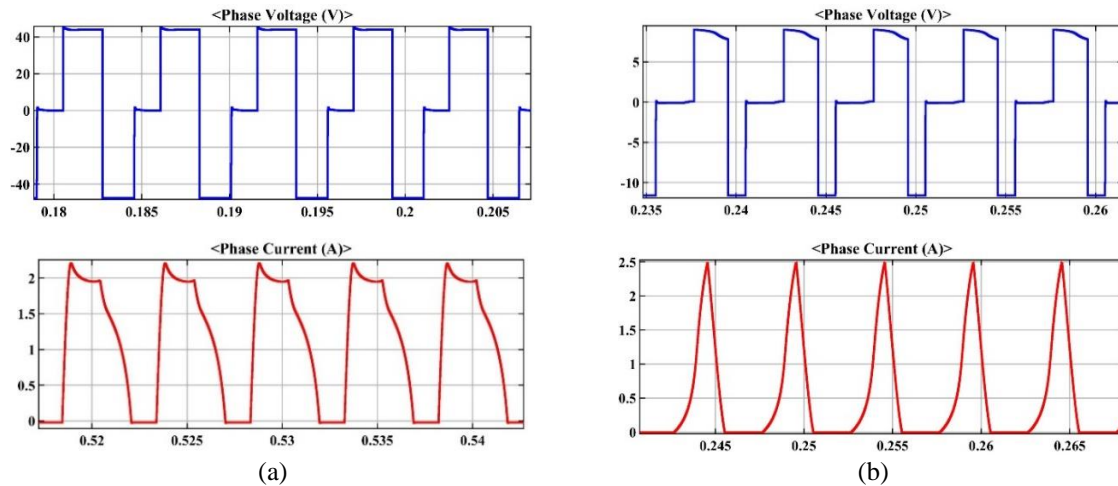


Figure 17. Simulation waveforms of the phase voltage and the phase current: (a) motoring mode at the motor speed n=1500 rpm, TL=0 Nm; and (b) generating mode at the n=1500 rpm, TL=0.65 Nm

The following Figure 18(a) and Figure 18(b) present experimental waveforms of the one-phase voltage and the one-phase current in motoring mode and generating mode. Figure 18(a) illustrates for the motoring mode (I quadrant) from top to bottom the experimental waveforms of the one-phase voltage and the one-phase current at $\theta_{on} = 24.13^\circ$, $\theta_{off} = 42.274^\circ$, torque load TL=0Nm and speed n=1500 rpm. Figure 18(b) illustrates the experimental waveforms of the same quantities for the generating mode (II quadrant)-from top to bottom waveforms of the one-phase voltage and the one-phase current at $\theta_{on} = 3.63^\circ$, $\theta_{off} = 20.87^\circ$, torque load TL=0.65 Nm and speed n=1500 rpm.

The next Figure 19(a) and Figure 19(b) present simulation waveforms for the motor speed at the operation in the first and second quadrants respectively. Figure 20(a) and Figure 20(b) illustrate the simulation results of the total torque T_e at the operation of the SRM in motoring and generating mode respectively. The following Figure 21(a) and Figure 21(b) show the simulation results of the one-phase inductance at the operation of the SRM in the first and second quadrants respectively. Table 2 and Table 3 summarize the comparison between simulation and experimental results for the two operation modes. The relative error between simulation and experimental results is within 5-10%. The differences between them are mainly due to the inaccuracy in the measurement of the angular position, emerging electromagnetic processes, noise and vibration when the phase winding is excited.

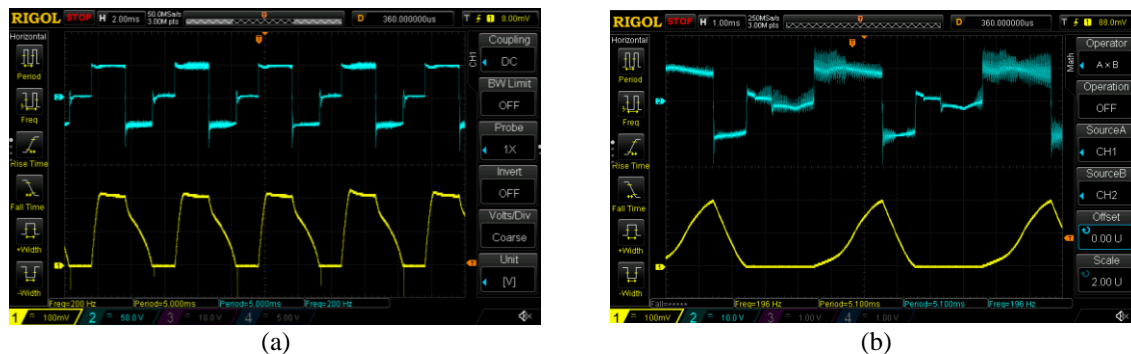


Figure 18. Experimental waveforms of the phase voltage and the phase current, (a) motoring mode at the motor speed n=1500 rpm, the torque load TL=0 Nm and (b) generating mode at the n=1500 rpm, TL=0.65 Nm

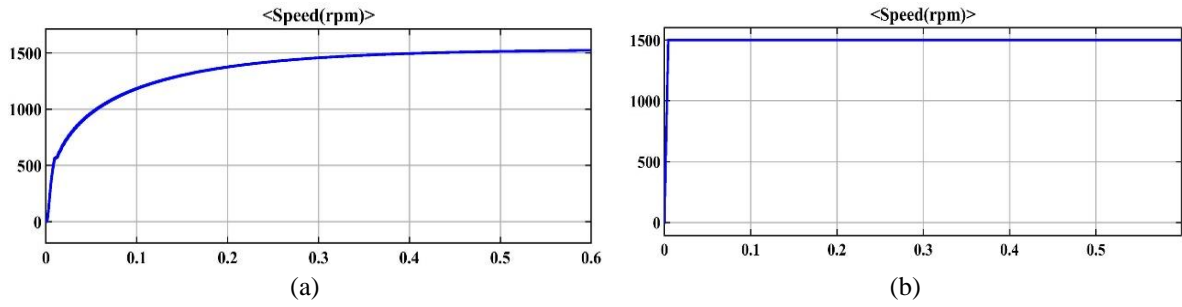


Figure 19. Simulation results of the motor speed at operation in: (a) the first quadrant and the torque load is $TL=0$ Nm and (b) the second quadrant and the $TL=0.65$ Nm

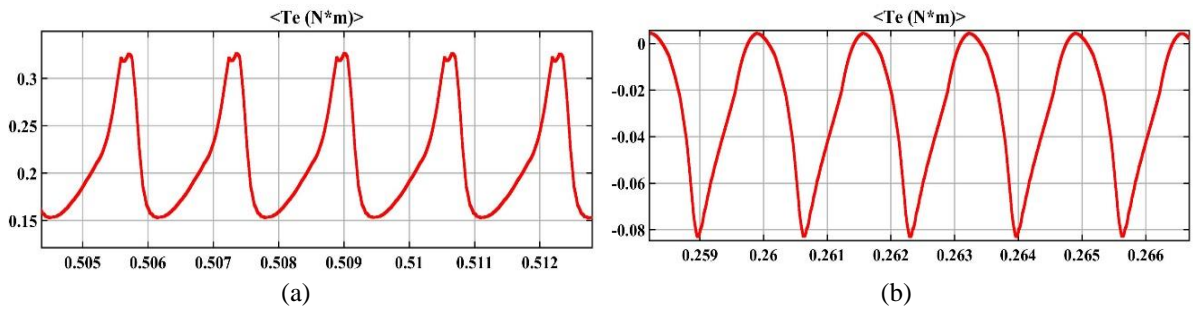


Figure 20. Simulation results for the total torque T_e at operation in: (a) motoring mode at the motor speed $n=1500$ rpm, the torque load $TL=0$ Nm and (b) generating mode at the $n=1500$ rpm, $TL=0.65$ Nm

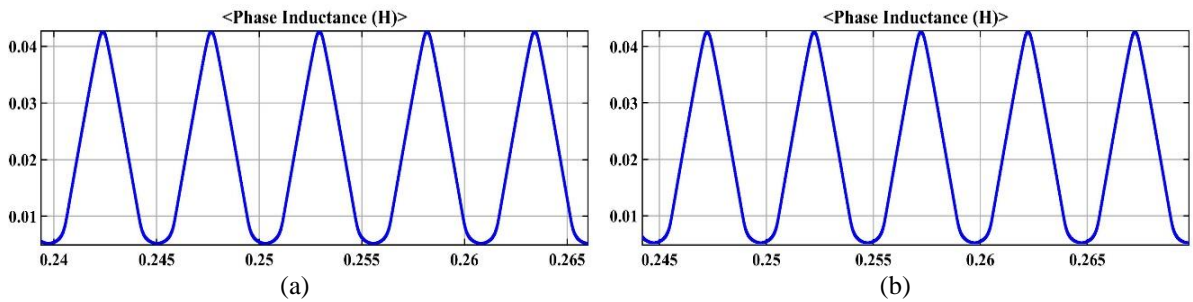


Figure 21. Simulation results of one-phase inductance: (a) first quadrant at the motor speed $n=1500$ rpm, the torque load $TL=0$ Nm and (b) second quadrant at the $n=1500$ rpm, $TL=0.65$ Nm

Table 2. A comparison between simulation and experimental results in the motoring mode (I quadrant)

	Turn-on angle θ_{on}	Turn-off angle θ_{off}	Speed, rpm	Phase voltage [V]	Phase current [A]	Total torque T_e [Nm]
Experimental results	24.13	42.274	1500	48	2.05	0.31
Nonlinear model simulation results	25.3	43.44	1500	45	2.02	0.305
Relative error, %	-4.85	-2.75	0	6.25	0.97561	1.61

Table 3. A comparison between simulation and experimental results in the generating mode (II quadrant)

	Turn-on angle θ_{on}	Turn-off angle θ_{off}	Speed, rpm	Phase voltage [V]	Phase current [A]	Total torque T_e [Nm]
Experimental results	3.63	20.87	1500	10	2	-0.059
Nonlinear model simulation results	3.8	20.944	1500	9	2.2	-0.065
Relative error, %	-4.68	-0.35	0	10	-10	-9.83

4. CONCLUSION

The paper describes a nonlinear three-phase 12/8 switched reluctance machine model suitable for use in a MATLAB/Simulink environment. To build the model, two-dimensional tables (look-up tables) obtained using the finite element analysis method and the Infolytica Motorsolve software simulator are used. The data for the look-up tables in excel files are entered using the source code for reading data in the Simulink software simulator. In order to ensure the model's reliability, 2D graphs of the simulation results from the FEM analysis and those generated from the MATLAB/Simulink are compared. A subsystem (block subsystem), where the user interface (mask) sets the necessary input parameters such as a phase resistance (Ω), a friction coefficient (N.m.s) and inertial value (kg.m.m) was created. Furthermore, an additional block has been added in the proposed model to monitor the inductance profile during the simulation study. A series of simulation and experimental results are derived to verify the accuracy of the built three-phase, 12/8 SRM (H55PWBM-1844) nonlinear model. A very good parity between simulation and experimental results is observed. The relative error between simulation and experimental results is within 5-10%.

ACKNOWLEDGEMENTS

The authors would like to thank the Research and Development Sector at the Technical University of Sofia for the financial support.

REFERENCES

- [1] R. Krishnan, "Application Considerations and Applications," in *Switched reluctance motor drives: modeling, simulation, analysis, design, and applications*, J. D. Irwin, Ed., 1st ed. Boca Raton, Florida, USA: CRC Press, 2001, 9, pp. 408–416.
- [2] M. Ahmad, "Switched Reluctance Motor Drives (SRM)," in *High Performance AC Drives Modelling Analysis and Control*, Berlin, Germany: Springer-Verlag Berlin and Heidelberg GmbH & Co. KG, 2010, ch. 6, pp. 129-159.
- [3] B. Bilgin, J. W. Jiang and A. Emadi, "Switched Reluctance Motor Drives Fundamentals to Applications," Boca Raton, Florida, USA: CRC Press, 2018.
- [4] A. Krasovsky, "Investigation of faulty behavior of the sensorless control switched reluctance motor drives," *International Journal of Power Electronics and Drive Systems*, vol. 12, no. 1, pp. 88-98, 2021, doi: 10.11591/ijpeds.v12.i1.pp88-98.
- [5] F. Soares and P. J. Costa Branco, "Simulation of a 6/4 switched reluctance motor based on Matlab/Simulink environment," *IEEE Transactions on Aerospace and Electronic Systems*, vol. 37, no. 3, pp. 989-1009, 2001, doi: 10.1109/7.953252.
- [6] R. Hasan, A. Hoque and A. Ahmed, "A Comprehensive Model of SRM in MATLAB Environment," *International Journal of Engineering and Computer Science*, vol. 12, no. 4, pp. 89-96, 2012.
- [7] D. K. Yankov, T. G. Grigorova and E. I. Dinkov, "Modeling of a Tree-Phase 12/8 Pole Switched Reluctance Motor in MATLAB," *IEEE XXVIII International Scientific Conference Electronics (ET)*, 2019, pp. 1-4, doi: 10.1109/ET.2019.8878654.
- [8] The MathWorks, "Model the dynamics of switched reluctance motor," 2022. [Online] Available: <https://www.mathworks.com/help/phymod/sps/powersys/ref/switchedreluctancemotor.html>.
- [9] B. Dong, "The modelling and simulation of 12/8 SRM and SRD Based on Simulink," *2nd International Conference on Electronic & Mechanical Engineering and Information Technology*, 2012, pp. 1373–1376, doi: 10.2991/emeit.2012.304.
- [10] N. Grebennikov and Z. Lebedev, "Development of Switched Reluctance Machines Model in MATLAB/Simulink," *Journal of Engineering and Applied Sciences*, vol. 11, no. 6, pp. 1434-1438, 2016, doi: 10.36478/jeasci.2016.1434.1438.
- [11] S. Saidani and M. Ghariani, "Static Simulation of a 12/8 Switched Reluctance Machine (Application: Starter-Generator)," *Intelligent Control and Automation*, vol. 6, no. 4, pp. 271-288, 2015, doi: 10.4236/ica.2015.64025.
- [12] H. Chen, Z. Zhang and Y. Xu, "Modeling, Simulation, and Experiment of Switched Reluctance Ocean Current Generator System," *Advances in Mechanical Engineering*, vol. 2013, no. 261241, pp. 1-14, 2013, doi: 10.1155/2013/261241.
- [13] X. Wang, R. Palka and M. Wardach, "Nonlinear Digital Simulation Models of Switched Reluctance Motor Drive," *Energies*, vol. 13, no. 24, pp. 1-17, 2020, doi: 10.3390/en13246715.
- [14] K. I. Hwu, "Applying POWERSYS and SIMULINK to Modeling Switched Reluctance Motor," *Institute of Electrical Engineering, National Taipei University of Technology*, vol. 12, no. 4, pp. 429-438, 2009, doi: 10.6180/jase.2009.12.4.07.
- [15] M. Hamouda and L. Számel, "Modeling and Simulation of Switched Reluctance Machines," in *Modelling and Control of Switched Reluctance Machines*, R. E. Araujo and J. R. Camacho, Eds. 1st ed. London, UK: IntechOpen, 2020, ch. 1, sec. 1, pp. 3–29, doi: 10.5772/intechopen.89851.
- [16] D. Yankov, "The finite element model and analyses of a three-phase 12/8 pole Switched Reluctance Motor," *21st International Symposium on Electrical Apparatus & Technologies (SIELA)*, 2020, pp. 1-4, doi: 10.1109/SIELA49118.2020.9167129.
- [17] A. Raj and P. Sreekanth, "Design of a Switched Reluctance Motor in Ansys Maxwell," *International Journal of Innovation Research in Science Engineering and Technology*, vol. 6, no. 2, pp. 2822-2826, 2017, doi: 10.15680/IJIRSET.2017.0602145.
- [18] D. Marcsa and M. Kuczmann, "Finite element analysis of switched reluctance motor with rotor position based control," *Pollack Periodica*, vol. 11, no. 3, pp. 153-164, 2016, doi: 10.1556/606.2016.11.3.14.
- [19] J. Faiz and S. Pakdelian, "Finite-element analysis of a switched reluctance motor under static eccentricity fault," *IEEE Transactions on Magnetics*, vol. 42, no. 8, pp. 2004-2008, 2006, doi: 10.1109/TMAG.2006.875997.
- [20] B. Ganji, M. Heidarian and J. Faiz, "Modeling and analysis of switched reluctance generator using finite element method," *Ain Shams Engineering Journal*, vol. 6, no. 1, pp. 85-93, 2015, doi: 10.1016/j.asej.2014.08.007.
- [21] Infologic Design Ltd, "Simcenter Motorsolve Electric Machine Design Software," [Online] Available: www.infologicdesign.co.uk.
- [22] P. Zhang, P. A. Cassani and S. S. Williamson, "An Accurate Inductance Profile Measurement Technique for Switched Reluctance Machines," *IEEE Transactions on Industrial Electronics*, vol. 57, no. 9, pp. 2972-2979, 2010, doi: 10.1109/TIE.2010.2048831.
- [23] R. Saxena, B. Singh and Y. Pahariya, "Measurement of Flux Linkage and Inductance Profile of SRM," *International Journal of Computer and Electrical Engineering*, vol. 2, no. 2, pp. 389-393, 2010, doi: 10.7763/IJCEE.2010.V2.166.

- [24] A. Shehata, Y. Abdalla, A. El-Wakeel and R. Mostafa, "Implementation of Switched Reluctance Motor, Measurement of Flux Linkage, and Inductance Characteristics," *Port-Said Engineering Research Journal*, vol. 21, no. 2, pp. 261-267, 2017, doi: 10.21608/pserj.2017.33375.
- [25] N. Radimov, N. Ben-Hail and R. Rabinovici, "Inductance measurements in switched reluctance machines," *IEEE Transactions on Magnetics*, vol. 41, no. 4, pp. 1296-1299, 2005, doi: 10.1109/TMAG.2005.844835.
- [26] J. Zhang and A. V. Radun, "A New Method to Measure the Switched Reluctance Motor's Flux," *IEEE Transactions on Industry Applications*, vol. 42, no. 5, pp. 1171-1176, 2006, doi: 10.1109/TIA.2006.880876.
- [27] Ž. Ferková, L. Suchý and J. Černohorský, "Measurement of switched reluctance motor parameters," *19th International Conference on Electrical Drives and Power Electronics (EDPE)*, 2017, pp. 287-290, doi: 10.1109/EDPE.2017.8123247.

BIOGRAPHIES OF AUTHORS



Dimitar Kirov Yankov     is currently working as an Assistant Professor at Department of Electronics, Faculty of Electronics and Automation at the Technical University of Sofia, Plovdiv Branch, Plovdiv, Bulgaria. He received his B.Eng. and M.Eng. degrees in Electronics Engineering from the Technical University of Sofia, Plovdiv Branch, Bulgaria, in 2014 and 2016 respectively. His research interests include the field of industrial electronics, power electronics, motor drives and renewable power energy. He can be contacted at email: d.yankov@tu-plovdiv.bg.



Tsvetana Grigorova     is currently working as an Associate Professor at the Department of Electronics, Faculty of Electronics and Automation at the Technical University of Sofia, Plovdiv Branch, Plovdiv, Bulgaria. She received the M.Eng. degree in Electronics and Automation, from the Technical University of Sofia, Sofia, Bulgaria, in 1991 and Ph.D. degree in Electronics converters from Technical University of Sofia in 2000. She has been an Associate Professor at Technical University of Sofia, Plovdiv Branch since 2008. Her research interests include different industrial applications such as power electronics converters for electrotechnological applications, motor drives, computer modelling and simulation of electronic circuits, and renewable power energy. She can be contacted at email: c_gr@tu-plovdiv.bg.